

## **Automated Measurement of Structures in CT and MR Imagery: A Validation Study**

Edward Ashton, Saara Totterman,  
Chihiro Takahashi  
*Department of Radiology  
University of Rochester  
edashton@ece.rochester.edu*

Jose Tamez-Pena, Kevin J. Parker  
*VirtualScopics, LLC  
parker@VirtualScopics.com  
tamez@VirtualScopics.com*

### ***Abstract***

*A novel method for the automated three-dimensional extraction and measurement of soft tissue lesions in CT imagery is presented. Extraction is carried out using a hybrid algorithm that incorporates elements from both competitive region growth and deformable template techniques. This algorithm is tested against manual tracing and shown to provide significantly improved performance using three performance metrics: speed, precision, and accuracy.*

## **1. Introduction**

The accurate measurement of soft tissue lesions and the tracking of small changes in lesions over time are topics of great interest both to pharmaceutical companies conducting drug trials and to clinicians attempting to monitor disease progression. Standard practice for obtaining such measurements currently involves either direct measurement taken from films or computer-aided manual tracing of lesion borders. Both of these processes are time consuming and prone to both inter- and intra-operator variation. We have developed a system, making use of a geometrically constrained region growth (GCRG) algorithm, for the automated identification and measurement of lesion boundaries. This algorithm combines elements of competitive region growth [1,2] and deformable template [3,4] techniques, and requires human interaction only for the initial location of the lesion.

Validation experiments have shown that this technique reduces human interaction time in the feature extraction process by approximately an order of magnitude. In addition, these experiments show a significant reduction in coefficient of variation for the automated system, with no appreciable loss in accuracy.

## **2. Experimental Procedure**

The initial experiment in this study involved two CT data sets – one abdominal and one head and neck scan, each containing a number of metastatic lesions. Two lesions from the abdominal study and one from the neck study were selected for analysis. Sub-images showing the lesions of interest are shown in Figure 1. Each of these lesions was traced manually in twenty separate trials by a single operator, then identified and extracted using the GCRG software in twenty separate trials, also by a single operator. Five descriptive parameters were calculated for each lesion in each trial: volume, maximum in-plane

surface area, maximum in-plane diameter, three-dimensional surface area, and maximum three-dimensional diameter. Because this experiment was intended to address questions of both speed and precision, timing statistics were also collected for each trial, both for user interaction and autonomous processing.

A second experiment, intended to further address questions of correlation between automated and manual methods, was carried out using magnetic resonance scans of a patient suffering from multiple sclerosis. This experiment is described fully in Section 4.

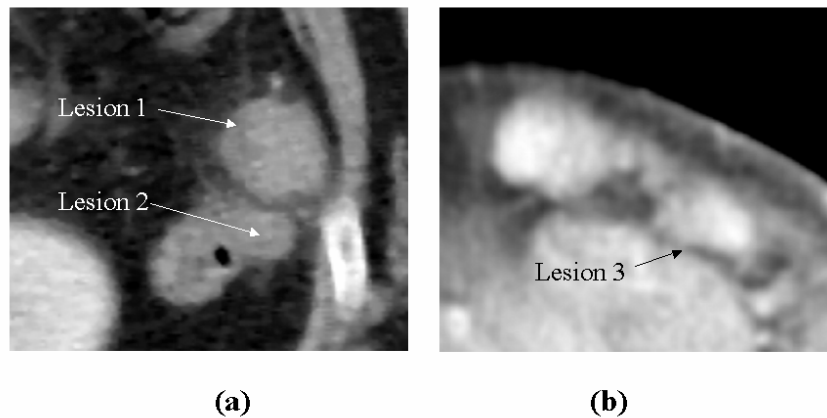


**Figure 1:** (a) Sub-image from abdominal scan containing two ovarian metastases. Note that the smaller lesion is attached to the bowel, and has no discernable edge in that region. (b) Sub-image from neck scan containing two tumors, one of which was analyzed for this experiment.

### 3. Methods

#### 3.1 Region extraction methods

Analysis in the experiments described here was carried out using software developed by VirtualScopics, a biomedical image analysis firm based in Rochester, NY. Manual extractions were obtained by tracing the border of each lesion on each image of the relevant scans with a computer mouse. The resulting three-dimensional structure was then automatically reconstructed and measured.

Automated extractions were carried out using VirtualScopics' GCRG algorithm. This software requires an operator to "seed" the structures of interest by clicking on an interior point. The seed region then expands into neighboring voxels provided that two constraints are satisfied: the grayscale value of the neighboring voxel must have a high probability of falling within the statistical distribution defined by all current included voxels, and inclusion of the neighboring voxel must not cause the shape of the included region to deviate excessively from the *a priori* regional shape model. This process continues until no further expansion is possible. The operation of this algorithm is illustrated in Figure 2.

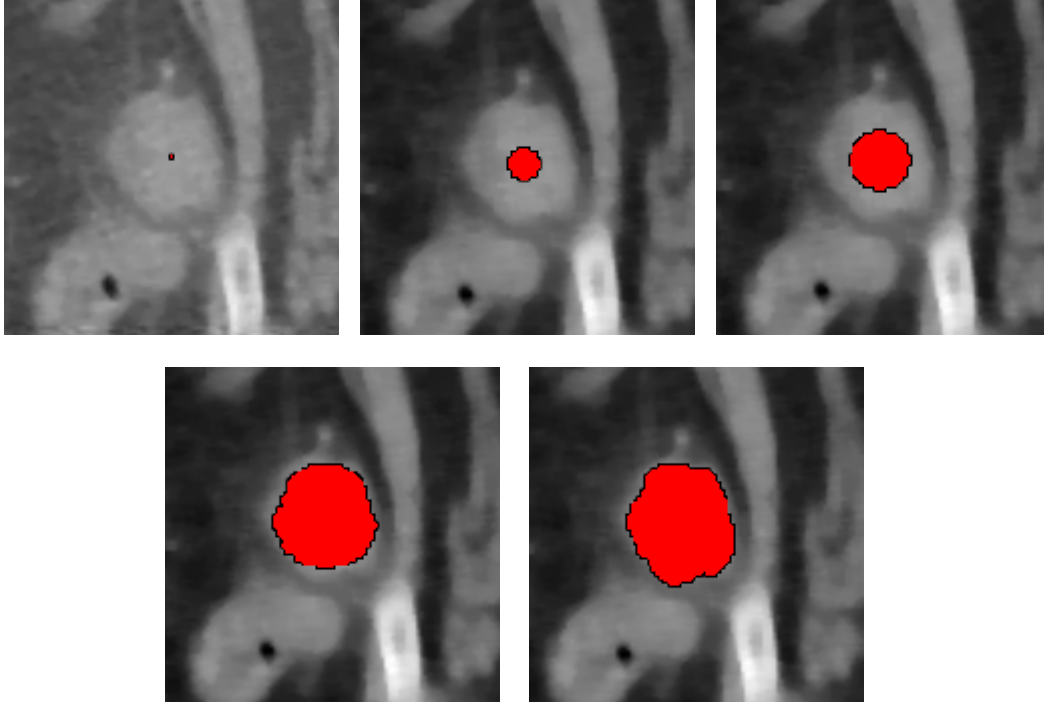


**Figure 2:** This image series shows the operation of the GCRG algorithm in the identification of the region boundary for Lesion 1 from Figure 1. The upper leftmost image shows the initial region seed. The lower rightmost image shows the final identified boundary.

### 3.2 Parameter measurement methods

Once region boundaries were identified either manually or automatically, a single set of algorithms was used to obtain parameter measurements. Volume and two-dimensional surface area were obtained through appropriately scaled voxel counts. Three-dimensional surface area and major axis length, however, are more complicated to obtain, and require somewhat more sophisticated methods of measurement.

The naïve assumption might be that 3-D surface calculation can be carried out through a summation of the areas of all exposed voxel faces. In fact, however, due to quantization errors at the object surface this method will grossly overestimate surface area. Our algorithm estimates the surface area of each exposed voxel using a formula based on the number and orientations of exposed faces. This method has been verified and works well on objects that are large relative to voxel size. All lesions in this study meet this criterion.

Measuring major axis length also seems at first glance to be a fairly simple problem. One simply needs to find the two most widely separated voxels in the data set and measure the distance between them. However, deciding which are the two most widely separated voxels in a particular off-axis direction is in fact not a trivial task. We accomplish this by first applying a K-L (principal components) transformation to the voxel set. Note that this is mathematically equivalent to calculating the moments of inertia for a solid object. This aligns the major axes of the object with the x, y, and z coordinate axes. We then measure the distance between the most widely separated voxels along each coordinate axis and call these distances the first, second and third major axes. This process is illustrated in Figure 3.

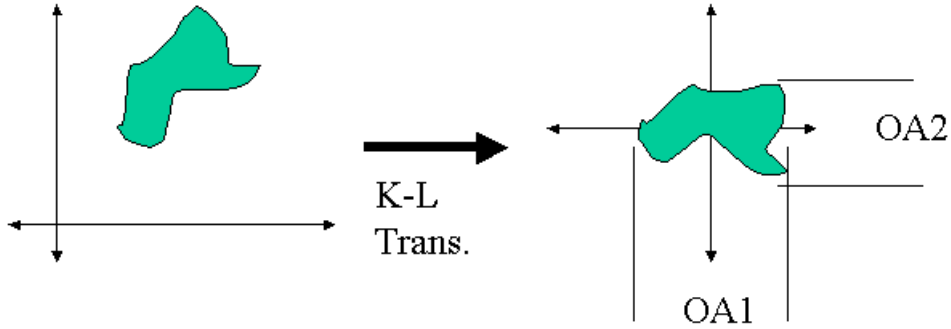


**Figure 3:** K-L Transform is used to obtain 1-D measurements.

## 4. Experimental results

### 4.1. CT cancer study

Our first experiment was intended to evaluate the performance of the automated measurement system with respect to three parameters: speed, precision, and accuracy. The results of the timing experiment are given in Table 1.

	Mean Human Time	Mean Proc. Time	Total
L1 & L2 Trace	4 min. 15 sec.	<1 sec.	4 min. 15 sec.
L1 & L2 GCRG	23 sec.	38 sec.	61 sec.
L3 Trace	3 min. 40 sec.	<1 sec.	3 min. 40 sec.
L3 GCRG	18 sec.	24 sec.	42 sec.

**Table 1:** Results of timing experiment. In each case human interaction time is reduced by approximately a factor of 10, while total processing time is reduced by approximately a factor of 4.

As expected, the automated system provides a significant reduction in both total processing time and, more importantly, human interaction time. This greatly reduces both the time and expense required to carry out a given study.

The second parameter, precision, is addressed in Table 2. This parameter is important for clinical trial applications in that it is directly related to the number of patients who must be enrolled in a given study in order to obtain statistically significant results. In a clinical setting, moreover, this parameter helps to determine the percentage change in a given structure that is required in order to determine that a particular treatment is or is not having the desired effect. This experiment shows that automated processing provides a

mean reduction in coefficient of variation with respect to manual processing of approximately 50%.

	Volume	2D Surf.	2D Major Axis	3D Surf.	3D Major Axis
L1 Tr.	6.84%	3.10%	3.90%	3.82%	3.52%
L1 GCRG	1.73%	2.34%	1.80%	1.70%	1.35%
L2 Tr.	5.09%	6.32%	5.13%	4.50%	5.87%
L2 GCRG	4.05%	6.16%	4.05%	3.83%	3.69%
L3 Tr.	3.28%	9.14%	3.07%	5.10%	1.47%
L3 GCRG	2.30%	2.70%	0.83%	2.55%	0.42%

**Table 2:** Results from precision experiment. Numbers shown are coefficients of variation for each parameter expressed as a percentage of the manually obtained mean. Automated processing shows consistently higher precision for all parameters.

The final parameter of interest is global accuracy. This is difficult to assess for this sort of study, which was carried out *in vivo*. However, one way to approach this question is to compare the results of the automated extraction to those of the manual extraction. The results of such a comparison are given in Table 3. These results are consistent with the error bars defined in Table 2.

	Volume	2D Surf.	2D Major Axis	3D Surf.	3D Major Axis
L1	5.25%	2.99%	6.70%	7.02%	7.95%
L2	5.03%	4.64%	2.58%	2.45%	10.18%
L3	4.32%	5.54%	6.81%	3.71%	0.29%

**Table 3:** Results from accuracy experiment. Numbers shown are difference between manual and automated extraction expressed as a percentage of the manually obtained value. Results are within expected error bars.

#### 4.2. MR multiple sclerosis study

Our second study was intended to further address the question of correlation between manual and automated parameter extraction results. To that end, a multi-spectral MR scan consisting of T1, T2, and proton density weighted images was obtained from a multiple sclerosis patient. 11 hypo-intense regions were identified in the T1 weighted images. These regions were first traced manually, then extracted using the GCRG algorithm. Manual and automated lesion extractions for one slice of this series are shown in Figure 4. Scatter-plots were then produced showing correlation between manual and automated extraction. These plots are given in Figure 5.

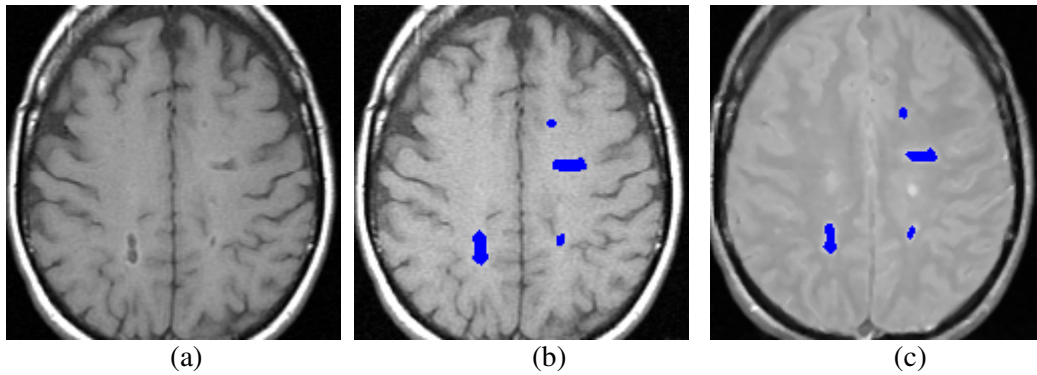


**Figure 4:** (a) One slice from the T1-weighted series used in this experiment. (b) Manually traced lesions from (a). (c) Automatically extracted lesions from (a).

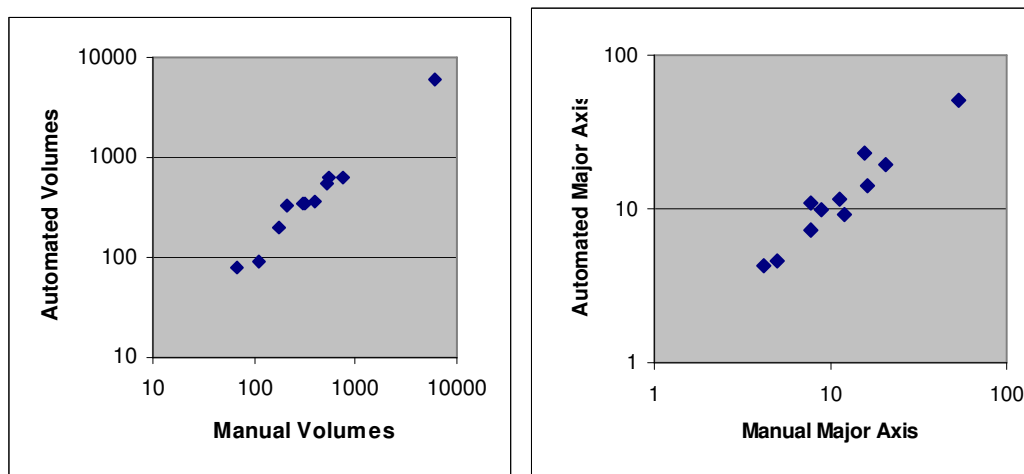


**Figure 5:** Scatter-plots showing correlation between manual and automated extraction for lesion volume and major axis calculations.

### 4.3 Experimental conclusions

The experiments carried out during the course of this study indicate that automated feature extraction of the sort described here provides significant advantages with respect to current manual or semi-automated techniques. Future work will include *in vitro* and animal studies, which should allow more definitive estimation of method accuracy.

## 5. References

- [1] "A Novel Volumetric Feature Extraction Technique with Applications to MR Images" E. Ashton, K. Parker, M. Berg, C. Chen, *IEEE Transactions on Medical Imaging*, vol. 16, no. 4, pp. 365 – 371 (1997).
- [2] "Image segmentation using globally optimum growth in three dimensions with an adaptive feature set" D. Taylor, W. Barrett, *Visualization in Biomedical Computing*, pp. 98 – 107 (1994).
- [3] "On active contour models and balloons" L. Cohen, *CVGIP: Graphical Models Image Processing*, vol. 53, pp. 211 – 218 (1991).
- [4] "3-D reconstruction from tomographic data using 2-D active contours" R. Chung, C. Ho, *Computers and Biomedical Research*, vol. 33, pp. 186 – 210 (2000).